ARTICLE

Magnetic Trapping of SH Radicals

J. S. Eardley[a], N. Warner[a,d], L. Z. Deng[c], D. Carty[a,b] and E. Wrede*[a]

Magnetic trapping of SH radicals, produced via the photostop technique, has been demonstrated. H_2S in a skimmed, supersonic molecular beam was photodissociated at 212.8 nm to produce SH inside a 330 mK deep static magnetic trap. The molecular-beam speed was controlled by the mixing ratio of H_2S in Kr to match the recoil velocity of the SH photofragments such that some SH radicals were produced with near-zero laboratory-frame velocity. The density of SH radicals in the $^2\Pi_{3/2}$, $v = 0$, $J = 3/2$ state was followed by (2+1) REMPI over seven orders of magnitude of signal intensity. 5 ms after photodissociation, SH radicals moving faster than the capture velocity of 13 m/s had left the trap. The 1/e trap lifetime of the remaining SH radicals was 40 ± 10 ms at an estimated density of 5×10^4 molecules/cm^3. Photostop offers a simple and direct way to accumulate absolute ground state molecules in a variety of traps.

Introduction

Following on from the successful field of cold and ultracold atoms, the field of cold and ultracold molecules has had some notable successes: quantum-state control of ultracold chemical reactions of KRb;[1] the first quantum simulation of many-body dynamics in spin lattices of KRb;[2] the lowest upper limit of the dipole moment of the electron;[3,4] molecule laser cooling;[5,6] magneto-optical trapping[7] and opto-electric cooling.[8]

Some experiments involved the indirect formation of ultracold molecules via the coherent association of ultracold atoms.[9,10] Such techniques are limited to combinations of atoms that can be laser cooled. Techniques that cool molecules directly strive to diversify the range of species that can be cooled. The molecular-synchrotron experiments[11] of Heiner *et al.* and the more recent laser-cooling[7] and opto-electric-cooling[8] experiments have reached sample temperatures on the order of 0.5 mK. However, the sub-milliKelvin barrier into the ultracold regime has yet to be significantly breached. Further cooling techniques are required to cool molecules directly towards 1 μK. A promising method is to use a refrigerant gas that can be cooled to ultracold temperatures and subsequently sympathetically reduce the temperature of molecules via elastic collisions.[12]

The key experimental step in sympathetic cooling is the trapping of the cold molecules such that they can be merged with the ultracold refrigerant gas. Parazzoli *et al.* attempted to sympathetically cool ND_3 with Rb. In this experiment, the

Stark-decelerated ND_3 was trapped electrostatically and the Rb was trapped magnetically.[13] Both atoms and molecules were not in their absolute ground states and sympathetic cooling was not possible due to fast inelastic processes that lead to trap loss. Apart from some exemptions that have been identified by theory, NH-Mg,[14] NH-Li[15] and CaH-Li/Mg,[16,17] trapped molecules should be in their absolute ground state, such that trap-ejecting inelastic collisions are energetically forbidden.

Trapping of ground-state ND_3 at 1 mK has been demonstrated in AC electrostatic traps,[18] but the translational energy due to molecule micromotion precludes sympathetic cooling.[12] This would not be an issue for optical-dipole traps and optical lattices, but such traps are shallow and have small volumes. Dipole traps, formed from standing waves of microwaves in a Fabry-Perot cavity, potentially have depths over 100 mK[19] and are a more promising starting point for sympathetic cooling.

The photostop method is capable of loading traps by producing the cold molecules directly inside the trap. This has been demonstrated with atomic bromine[20] in a permanent magnetic trap.[21] Following on from our work on the production of cold NO via photostop,[22] we demonstrate that cold SH radicals can be magnetically trapped following the photodissociation of H_2S in a molecular-beam.

Photostop technique

The photostop technique requires that the molecular-beam speed, v_{beam}, and the recoil speed of the desired photofragment are matched. Photofragments with a recoil velocity opposing the velocity of the precursor molecule are created at rest in the laboratory. This leads to the photostop condition

a. *Department of Chemistry, Joint Quantum Centre Durham-Newcastle, Durham University, South Road, Durham, DH1 3LE, U.K.*
   E-mail: eckart.wrede@durham.ac.uk
b. *Department of Physics, Joint Quantum Centre Durham-Newcastle, Durham University, South Road, Durham, DH1 3LE, U.K.*
c. *State Key Laboratory of Precision Spectroscopy, East China Normal University, Shanghai, 200062, People's Republic of China.*
d. *Current address: Diamond Light Source Ltd, Harwell Science & Innovation Campus, Didcot, OX11 0DE, U.K.*

$$v_{\text{beam}} = \sqrt{\frac{2m_{\text{H}}(h\nu - D_0 - E_{\text{int}})}{m_{\text{SH}}\,m_{\text{H}_2\text{S}}}}, \qquad (1)$$

in which $m_{\text{H}_2\text{S}}$ is the mass of the precursor, m_{SH} the photostopped fragment and m_{H} the co-fragment, $h\nu$ is the photon energy of the dissociation laser, D_0 is the threshold dissociation energy and E_{int} is the sum of the internal energies of both photofragments.

In principle, photostop is applicable to any precursor molecule with a dissociative absorption spectrum that is accessible via available laser sources and whose photostop condition for the desired fragment, according to Eqn (1), is achievable in a supersonic beam. Ideally, the state distribution of the photofragments is biased towards the desired quantum state.

Experiment

A skimmed, supersonic molecular beam of H_2S in Kr was generated by a solenoid valve (Parker, General Valve, Series 9) pulsed at 5 Hz with a measured pulse length (FWHM) of 120 μs at the trap centre and operated at 4 bar backing pressure. The H_2S photodissociation is well known and proceeds via a perpendicular transition from the $^1A_1$ ground to the $^1B_1$ excited state followed by predissociation through the $^1A_2$ state leading to SH($^2\Pi_\Omega$) and H(^2S) fragments.[23] The dissociation light was generated by a pulsed Nd:YAG laser (Continuum Surelite I-10, 5 ns pulse width). By quintupling the 1064 nm fundamental to 212.8 nm light a pulse energy of 1.5 mJ was produced. The photostop condition, Eqn (1), was met for $v_{\text{beam}} = 575$ m s^{-1} which was achieved through a H_2S to Kr mixing ratio of 3:1. The linear polarisation of the dissociation laser was arranged perpendicular to the molecular beam such that the torus-shaped angular distribution of the SH photofragments contained the molecular-beam axis. The resulting SH velocities ranged from zero to 1150 m s^{-1} in the direction of the molecular beam.

The measurements were performed in a purpose-built high-vacuum chamber pumped by two turbo molecular pumps, with a combined pumping speed of 1510 l s^{-1}, and a modified cryopump. The chamber base pressure, with the cryopump at its lowest temperature, was measured by a Bayard-Alpert gauge to be 10^{-9} mbar, the pressure was 10^{-6} mbar under running conditions.

The magnetic trap, as shown in Fig. 1, was formed by two NdFeB ring magnets (OD 12 mm, ID 4 mm, height 7 mm, bore 4 mm) in anti-Helmholtz configuration with a residual magnetisation of 1.46 T. The resulting trap had a volume of about 0.1 cm^3 and a depth of 0.41 T. SH($^2\Pi_{3/2}$, $v = 0$, $J = 3/2$) in its $M_J = +3/2$ low-field-seeking Zeeman sub-state possesses the largest Zeeman shift, which in this trap is equivalent to a depth of 330 mK and a capture velocity of 13 m s^{-1}. 60% of the SH fragments are produced in the trappable spin-orbit ground state ($^2\Pi_{3/2}$), of which (>95%) are in the vibrational ground state
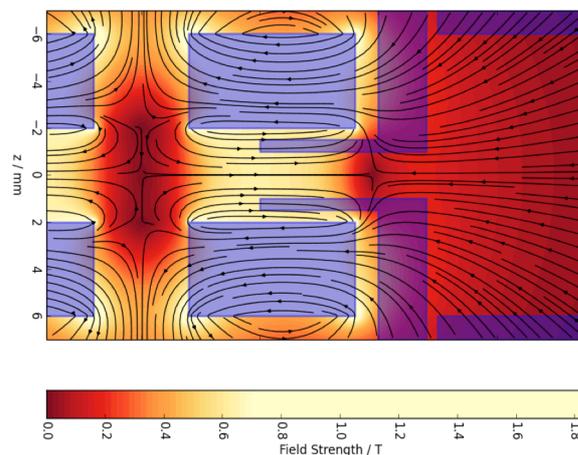
Fig. 1 2D cut through of the permanent magnetic trap formed by two NdFeB ring magnets in anti-Helmholtz configuration. The cylindrical symmetry axis is the x axis in the figure. The field strength is indicated by the colour gradient. The direction of the B-field is given by the black arrows. Note that both magnets are identical but the left magnet is cut by the figure. The ion extraction and TOF tubes are indicated in the right of the figure.

($v = 0$). A further 8% are in the lowest $J = 3/2$ rotational state.[23,24]

The magnetic trap was mounted to the second stage of the cryostat of the modified cryopump (Leybold-Heraeus, RPK 1500) and cooled to approximately 20 K, thus turning the magnets and their housing into pumping surfaces. A radiation shield surrounding the trap was cooled by the first stage of the cryostat to 80 K, which provided additional pumping via activated charcoal on internal surfaces. The skimmer (Beam Dynamics, Model 40.5, 2 mm orifice) was mounted on a plate, which guided the majority of the unskimmed beam towards the primary turbo pump, approximately 4 cm downstream from the pulsed valve. This setup resulted in quasi-differential
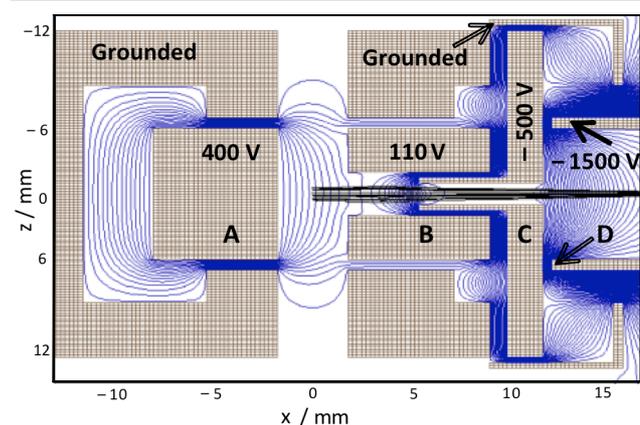
Fig. 2 SIMION 8.0 simulation showing a cut through of the cylindrically symmetric electrodes for ion extraction from the trap. (A) Ring magnet with copper insert, (B) opposing ring magnet, (C) extractor, (D) time-of-flight tube. Blue lines show the electrostatic potential contours and black lines show simulated ion trajectories from within the probe volume.

pumping that maintained the best vacuum possible in the magnetic trapping region. As explained later, these measures were essential to minimise background H_2S gas.

The photofragments were detected by (2+1) resonance-enhanced multiphoton ionisation (REMPI) using the $[a\,{}^1\Delta]\,3d\pi\,{}^2\Phi \leftarrow\leftarrow \tilde{X}\,{}^2\Pi_{3/2}\,(v''=0)$ transition.[25] The probe light was generated by a frequency-doubled, Nd:YAG pumped dye laser (Sirah, CobraStretch with Coumarin 503 (307) dye; Continuum, Surelite I-10, 10 Hz repetition rate). Typically 1 mJ of probe light was focussed to an approximate spot size of diameter 200 µm at the centre of the trap to probe via the S_1 ($J = 3/2$) line at 255.75 nm.

In a bespoke setup, the permanent magnets and the trap housing also provided the ion extraction fields, see Fig. 2. The bore of one magnet was filled with a copper insert and the other was left open to allow for ion extraction through the 4 mm hole of the magnet. In combination with an extractor tube protruding into the bore of the magnet and a time-of-flight (TOF) tube, the ions were guided to a dual micro-channel plate (MCP) detector (Hamamatsu, F12334-11). The size of the focused probe laser convoluted with the ion extraction volume gave an effective probe volume of $1.5{\times}10^{-3}$ cm^3. This accounted for approximately 2 % of the trap volume. The TOF signal attributable to SH ions was approximately 20 ns wide, as shown in Fig. 3, and was well separated from H_2S ion signal.

The signal from the MCP detector was recorded on a digital oscilloscope (Lecroy, Waverunner 610Zi, 1 GHz, 10 GS/s) and divided by the dissociation and probe laser intensities, recorded by pyroelectric detectors (Sensor-und Lasertechnik, PEM 21) to give

$$S_{\text{tot}} = \frac{S_{\text{MCP}}}{I_{\text{probe}}^q \cdot I_{\text{diss}}^p}, \qquad (2)$$

in which S_{tot} is the REMPI signal and S_{MCP} is the integrated or event-counting signal from the MCP. I_{probe} and I_{diss} are the intensities of the probe and dissociation lasers, respectively and q and p represent the power dependencies of the REMPI signal on the two lasers, measured to be 2.2 and 1.0, respectively.

The focussed probe light can also photodissociate H_2S at 255.75 nm. At delays greater than 5 ms between the dissociation and probe lasers, the signal attributable to the 255.75 nm photodissociation of background H_2S in the trap was often greater than the signal due to photostopped SH radicals. To confidently measure the photostopped SH molecules, the dissociation laser was triggered with every other molecular-beam pulse to allow shot-to-shot background subtraction. The photostop signal, S_{bgsub}, was given by

$$S_{\text{bgsub}} = S_{\text{tot}} - S_{\text{bg}}. \qquad (3)$$

Results
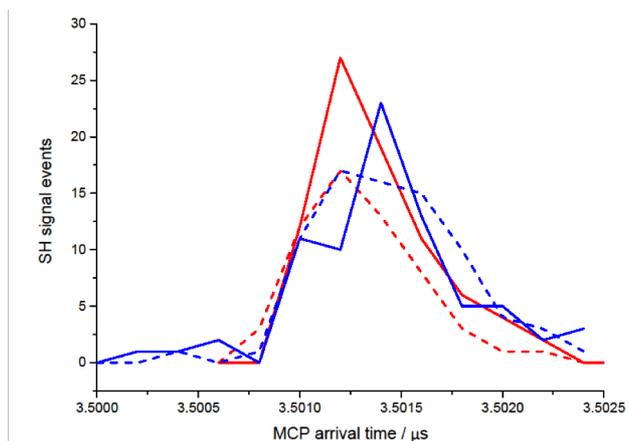
Fig. 3 Time-of-flight distributions of detected SH ions (histogram bin width 2 ns). Total signal, S_{tot}, recorded with both dissociation and probe lasers (solid lines) and background signal, S_{bg}, recorded with probe laser only (dashed lines). The difference yields the background–subtracted SH signal, S_{bgsub}, as plotted in Fig. 4. Measurements with the magnetic trap at 11 ms delay (red lines) and without a trapping field at 10 ms delay (blue lines).

The relative number of SH radicals inside the probe volume was followed as a function of the time delay between the dissociation and probe lasers. With increasing delay, fewer SH radicals were detected as fast SH fragments left the probe volume and after 5 ms only trapped ones remained. The SH signal was normalised against the maximum signal at "zero delay" (10 ns) to account for day-to-day fluctuations in the molecular-beam source. As the signal intensity decreased, the gain of the MCP detector was adjusted to further amplify the signal. In this way, S_{bgsub} could be followed over seven orders of magnitude.

The error in S_{bgsub} became significant when the number of SH radicals was low enough to require event counting for signal collection. The best estimate of the error in the background subtracted signal is given by
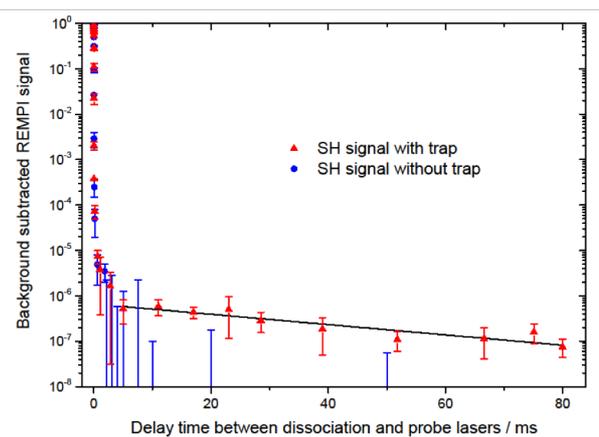
Fig. 4 Background-subtracted signal as a function of delay between dissociation and probe lasers, error bars are one standard error. Red triangle points: with a trapping magnetic field potential. Black line: linear regression of trapping data with a delay greater than 5 ms showing a 1/e lifetime of 40 ± 10 ms. Blue circle points: without a trapping magnetic field potential. Some blue error bars are without associated points, this was due to the photostopped SH signal becoming immeasurably small compared to the background.

in which N_{signal} and $N_{background}$ are the number of counted events attributed to photostopped SH signal and H_2S background and f_{laser} is the small constant fractional error associated with the variation in the laser powers. Thus a background subtracted measurement was statistically significant if N_{signal} exceeded $\sqrt{N_{background}}$. To measure S_{bgsub} at delays greater than 5 ms a minimum of 30000 acquisitions were required for each delay time.

The measurement was repeated without a permanent trapping potential. To achieve this, the magnets were replaced with 'magnots.' These copper rings provided no trapping potential to the SH radicals. Fig. 3 demonstrates the successful trapping of photostopped SH radicals. There is only a statistically significant background-subtracted SH signal present with the magnetic trap installed. The decay curves with and without magnets are shown in Fig. 4. Without a trapping field after a 3 ms delay, S_{tot} and S_{bg} became too similar to confidently distinguish a difference between them causing the exploding error bars. The magnetically trapped SH radicals were measured for up to 80 ms delay time and showed a 1/e trap lifetime of 40 ± 10 ms by the fitting of data points above 5 ms delay. This lifetime is short compared to other trapping experiments and is almost certainly limited by elastic and inelastic collisions in the trapping region with a significant density of background gas, particularly H_2S, which produces the one-colour background signal from the probe laser alone.

We estimate a H_2S number density at the moment of photodissociation of 10^{14} cm^{-3} based on the dynamics of supersonic expansions.[26] Given the dissociation laser peak intensity of 7.5 MW/cm^2 across the molecular beam, the H_2S absorption cross section of 2.4×10^{-18} cm^2 at 212.8 nm and unity dissociation yield we estimate the total SH density to be 2×10^{12} cm^{-3}. 5 % of the SH radicals are produced in the correct spectroscopic state,[24] making the maximum measured photostop signal equivalent to 9×10^{10} cm^{-3}. The intercept of the linear fit at zero time delay in Fig. 4 shows that 0.6 ppm of the probed SH photofragments are created in the correct conditions for trapping, this leads to a density of 5×10^4 cm^{-3} of trapped SH in the +3/2 and +1/2 Zeeman sub-states.

Conclusions

With these experiments, we demonstrate that photostop can produce trapped atomic[21] and molecular radicals.

So far, the SH radical number density is only an estimate. It could be verified using cavity-enhanced laser-induced fluorescence (CELIF) in a similar way to Mizouri *et al.*[27] Calibration of the REMPI signal at high densities would yield an absolute density of trapped SH radicals.

Although the estimated trap density achieved here is low, this does not preclude sympathetic cooling in a vast excess of refrigerant atoms and combining photostop with a microwave trap will result in no foreseeable additional losses. The modest molecular-beam source used could be improved, yielding up to a factor of ten increase in the number of trapped radicals. Additionally, a magnetic trap with a smaller volume and greater potential gradient would increase the trapped SH

$$\delta S_{bgsub} = S_{bgsub} \sqrt{\left(\frac{1}{\sqrt{N_{signal}}}\right)^2 + \left(\frac{\sqrt{N_{background}}}{N_{signal}}\right)^2 + (f_{laser})^2}, \qquad (4)$$

density. The modest trapping lifetime could be increased by improved differential pumping and by using a shorter and higher-density molecular beam pulse to minimise the amount of background gas in the trap.

Photostop could be used to slow and trap other species such as SO, CN, Cl, I and ($^3P_2$) oxygen atoms. In particular the photostop of O($^3P_2$)[28] from NO_2 could achieve trapped cold atom densities greater than 1×10^7 cm^{-3} with an improved source. One of our aims is to demonstrate the accumulation of trapped species. This should be possible by increasing both the trapping density and lifetime such that species remain trapped until the next photostop event.

Potentially the sympathetic cooling of triplet oxygen with ultracold Rb atoms could lead to an indirect cooling method for creating ultracold RbO (estimated electric dipole moment of 8.5 D) by coherent association of the ultracold atoms.

Acknowledgements

Notes and references

1. Ospelkaus, S., Ni, K. K., Wang, D., De Miranda, M. H. G., Neyenhuis, B., Quéméner, G., Julienne, P. S., Bohn, J. L., Jin, D. S. & Ye, J, Science, 2010, **327**, 853–857.
2. Yan, B., Moses, S. A., Gadway, B., Covey, J. P., Hazzard, K. R. A., Rey, A. M., Jin, D. S. & Ye, J, Nature, 2013, **501**, 521–525.
3. Hudson, J. J., Smallman, K. I. J., Sauer, B. E., Tarbutt, M. R. & Hinds, E. A, Nature, 2011, **473**, 493-496.
4. Baron, J., Campbell, W. C., DeMille, D., Doyle, J. M., Gabrielse, G., Gurevich, Y. V., Hess, P. W., Hutzler, N. R., Kirilov E., Kozyryev, I., O'Leary, Panda, C. D., Parsons, M. F., Petrik, E. S., Spaun, B., Vutha, A. C. & West A. D, Science, 2014, **343**, 269–272.
5. Zhelyazkova, V., Cournol, A., Wall, T. E., Matsushima, A., Hudson, J. J., Hinds, E. A., Tarbutt, M. R. & Sauer, B. E, Phys. Rev. A, 2014, **89**, 53416.
6. Hummon, M. T., Yeo, M., Stuhl, B. K., Collopy, A. L., Xia, Y. & Ye, J, Phys. Rev. Lett., 2013, **110**, 143001.
7. Steinecker, M. H., McCarron, D. J., Zhu, Y. & DeMille, D, ChemPhysChem, 2016, **17**, 3664–3669.
8. Prehn, A., Ibrügger, M., Glöckner, R., Rempe, G. & Zeppenfeld, M, Phys. Rev. Lett., 2016, **116**, 63005.
9. Molony, P. K., Gregory, P. D., Zhonghua, J., Lu, B., Köppinger, M. P., Le Sueur, C. R., Blackley, C. L., Hutson, J. M. & Cornish, S. L, Phys. Rev. Lett., 2014, **113**.
10. Shimasaki, T., Bellos, M., Bruzewicz, C. D., Lasner, Z. & DeMille, D, Phys. Rev. A, 2015, **91**, 021401.

11. Heiner, C. E., Carty, D., Meijer, G. & Bethlem, H. L, Nat. Phys., 2007, **3**, 115–118.
12. Lim, J., Frye, M. D., Hutson, J. M. & Tarbutt, M. R, Phys. Rev. A, 2015, **92,** 053419.
13. Parazzoli, L. P., Fitch, N. J., Żuchowski, P. S., Hutson, J. M. & Lewandowski, H. J, Phys. Rev. Lett., 2011, **106**, 193201.
14. Wallis, A. O. G. & Hutson, J. M, Phys. Rev. Lett., 2009, **103**, 183201.
15. Wallis, A. O. G., Longdon, E. J. J., Żuchowski, P. S. & Hutson, J. M, Eur. Phys. J. D, 2011, **65**, 151–160.
16. Tscherbul, T. V., Kłos, J. & Buchachenko, A. A, Phys. Rev. A, 2011, **84**, 040701.
17. Warehime, M. & Kłos, J, Phys. Rev. A, 2015, 92, 32703.
18. van Veldhoven, J., Bethlem, H. L. & Meijer, G, Phys. Rev. Lett., 2005, **94,** 083001.
19. Dunseith, D. P., Truppe, S., Hendricks, R. J., Sauer, B. E., Hinds, E. A. & Tarbutt, M. R, J. Phys. B At. Mol. Opt. Phys., 2015, **48**, 45001.
20. Doherty, W. G., Bell, M. T., Softley, T. P., Rowland, A., Wrede, E., Carty, D, Phys. Chem. Chem. Phys., 2011, **13**, 8441–8447.
21. Rennick, C. J., Lam, J., Doherty, W. G. & Softley, T. P, Phys. Rev. Lett., 2014, **112,** 023002.
22. Trottier, A., Carty, D. & Wrede, E, Mol. Phys., 2011, **109**, 725–733.
23. Weiner, B., Levene, H., Valentini, J. & Baronavski, A, J. Chem. Phys., 1989, **90**, 1403–1414.
24. Morley, G., Lambert, I., Mordaunt, D., Wilson, S., Ashford, M., Dixon, R. & Western, C, J. Chem. Soc.-Faraday Trans., 1993, **89**, 3865–3875.
25. Milan, J. B., Buma, W. J. & deLange, C. A, J. Chem. Phys., 1996, **105**, 6688–6712.
26. Scoles, G., Bassi, D., Buck, U. & Laine, D. C, Atomic and Molecular Beam Methods, Vol. 1 (Oxford University Press, 1988).
27. Mizouri, A., Deng, L. Z., Eardley, J. S., Nahler, N. H., Wrede, E., Carty, D, Phys. Chem. Chem. Phys., 2013, **15**, 19575–19579.
28. Matthews, S. J., Willitsch, S. & Softley, T. P, Phys. Chem. Chem. Phys., 2007, **9**, 5656–5663.
29. Supporting data are available under open access through Durham University Collections at https://doi.org/10.15128/r2ft848q61p .